

Analytical, Simulation and Measurement Studies of a Dual-Band Open-Sleeve Curved Meander Line Antenna on a Flexible Substrate

Elodie Georget*, Redha Abdeddaim, and Pierre Sabouroux

Abstract—An innovative antenna on flexible substrate with two resonators is presented. The antenna is composed of a metallic wire sewn on the substrate. Two dipolar modes in far field are radiated. To understand the interaction of the resonators with the principal antenna, studies with and without the sleeves are done in near field and far field.

1. INTRODUCTION

The growing demands for greater capacities, broadband service, and communication speeds to transmit data in embedded system like mobile phone [1], security [2] and RFID systems [3] has imposed working on new types of antennas. In order to respond to these new constraints, these antennas should be wideband, or multiband and embedded to all types of environments. They must be light weight, low profile, highly flexible, have a high impact and a simple structure. This has resulted in new antenna designs [4], like fractal antennas [5, 6] for wideband or multiband systems, meander elements [7–9], or open-sleeve antennas [10–13] for multiband frequencies. To reduce the volume of the antennas, flexible substrate [14–20] are used.

In this paper, the goal is to design an innovative antenna on a flexible substrate. This antenna has to be folded and inserted in an embedded system. The antenna deploys when the embedded system is used once deployed.

To realize this antenna, we present a new method to design a compact and flexible dual-band dipole antenna. This is based on the coupling of several resonators. We start this study with a simple monopole antenna which radiates a dipole and quadrupole mode at its first f_1 and second f_2 frequency respectively [21]. We transform the far field radiation of the second mode into a dipolar mode by adding two parasitic elements. The length and the position of the parasitic elements are studied to resonate at the second mode. This antenna is called an open-sleeve monopole antenna. This configuration is validated by measurements and simulations in near field and far field domains.

2. DESCRIPTION OF THE ANTENNA

A monopole antenna with ground plane was realized (Figures 1(a)–(b)). Thanks to image theory [22], this antenna radiates as a dipole device. The radiating element consists on a meander monopole line. It was chosen in order to reduce the length of the antenna [7, 8]. This driven element is formed of two wires sewn in zigzag, a metallic wire of diameter $d = 0.30$ mm and a classical cotton wire. Due to the used technique to realize the monopole, the radiating element is not a perfect meander, but a curved

Received 20 December 2013, Accepted 11 February 2014, Scheduled 18 February 2014

* Corresponding author: Elodie Georget (elodie.georget@fresnel.fr).

The authors are with the Aix Marseille Université, CNRS, Centrale Marseille, Institut Fresnel, UMR 7249, Campus Universitaire de Saint Jérôme, Marseille 13013, France.

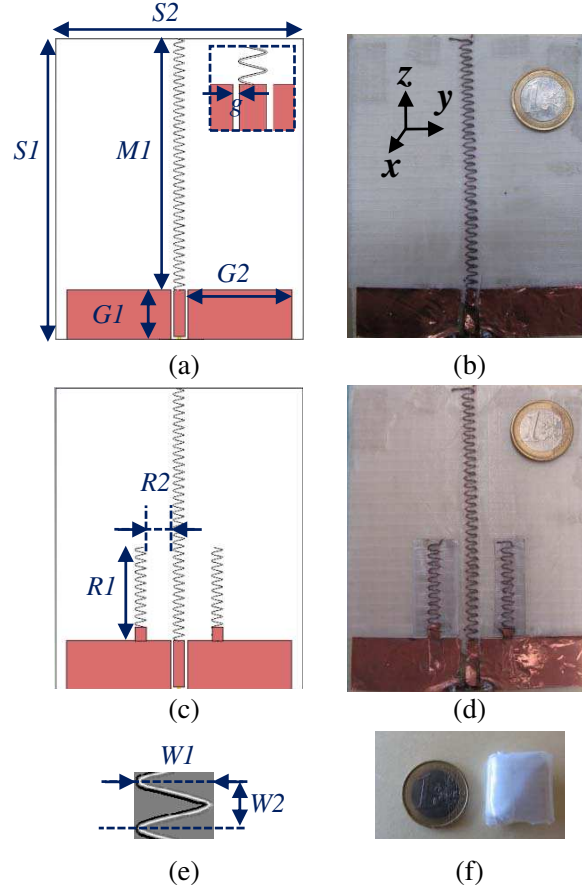


Figure 1. (a) Curved meander line antenna design ($S1 = 110$; $S2 = 90$; $M1 = 92$; $G1 = 18$; $G2 = 38$; $g = 2$). (b) Realization of the antenna (a). (c) Open-sleeve curved meander line antenna design ($R1 = 34$; $R2 = 9$). (d) Realization of the antenna (c). (e) Sinusoidal curve of the metallic wire ($W1 = 4$; $W2 = 2.7$). (f) Used space when the antenna is folded. All dimensions are in mm.

meander line because the zigzag seam is not tight. This curved meander line can be approximated as a sinusoidal curve $l(z)$:

$$l(z) = \frac{W1}{2} * \sin\left(\frac{2\pi}{W2} * z\right) \quad (1)$$

with $W1 = 4$ mm the width of the driven element and $W2 = 2.7$ mm the period of the sine. The length of the driven element is $M1 = 0.6 * (\lambda_1/4) = 92$ mm and permits to gain 40% compared to a quarter wavelength monopole line. This monopole is fed by a coplanar line (which extends the radiating element). In order to gain space, the ground plane ($M1$) composed of copper tape is chosen to be planar. In the second time, two parasitic elements manufactured in the same way as the primary radiator are added on each side of the driven element (Figures 1(c)–(d)). They are connected to the ground plane by a copper tape. Their size is chosen to resonate at the second mode of the curved meander line antenna. This is equal to $R1 = 0.6 * (\lambda_2/4) = 34$ mm. The distance between the monopole and the parasitic is $R2 = 9$ mm. This antenna is called the open-sleeve curved meander line antenna.

The resonance frequency of a monopole antenna printed on a substrate of relative permittivity ϵ_r^* is equal to [22]:

$$f = \sqrt{\epsilon_r^*} \frac{c}{\lambda_0} \quad (2)$$

with c the speed of light in vacuum and λ_0 the wavelength in free space of the fundamental mode. The permittivity of the used substrate $\epsilon_r^* = (2.70 - j0.04)$ of thickness $h = 0.0875$ mm was characterized to

reduce the discrepancy at the resonance frequencies of the antenna [23–25]. Figure 1 shows the image of the realized and simulated with CST Microwave Studio antenna with and without the resonators.

3. NUMERICAL AND EXPERIMENTAL RESULTS

3.1. Determination of the Resonance Frequencies

The measured reflection coefficients S_{11} of the monopole antenna and of the open-sleeve antenna are displayed in Figure 2 to characterize the matching of the antenna. The curved meander monopole antenna radiates the dipole mode at $f_1 = 470$ MHz and the quadrupole mode at $f_2 = 1330$ MHz. When the parasitic elements are added, they behave like a matching circuit for the first resonance frequency. The antenna is 5 dB better matched at 450 MHz. The second resonance frequency shifted in lower frequency at 1170 MHz with a 1.5 dB better matching due to the coupling between the parasitic elements and the monopole element.

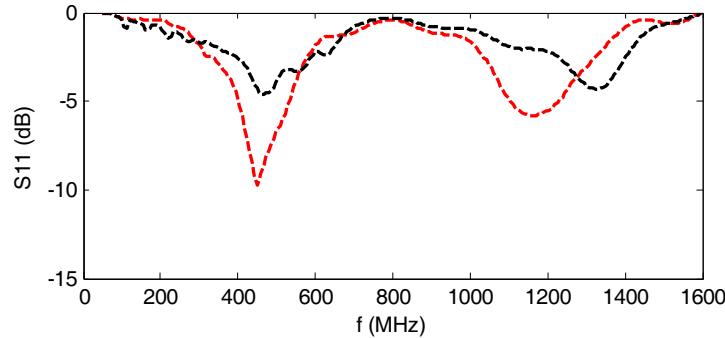


Figure 2. Measured reflection coefficient S_{11} of the curved meander line antenna with (red line) and without (black dashed line) the two resonator elements.

3.2. Near Field Results

In order to understand the far field radiating of the antennas, the near field is studied. The distribution current along the antenna provides a significant description of the radiation. The complexity of the elementary geometry of the antenna on the one hand and low thickness of the metallic wire on the other hand makes the measurement of current very difficult. To solve this problem, we developed a setup to measure the magnetic field. The measurement of the magnetic field is directly proportional to the current distribution. The equation that relates the magnetic field at a studied point $H(x)$ to the current distribution in the studied space $J(x')$ [21] is:

$$H(x) = \frac{1}{\mu_0} \nabla \times \left(\frac{\mu_0}{4\pi} \int J(x') \frac{e^{ik|x-x'|}}{|x-x'|} d^3x' \right) \quad (3)$$

with μ_0 the permeability of free space, k the wavenumber, x the studied point, and x' a point in the studied space. In regard of this equation, we decided to measure the y component of the magnetic field. The study of the magnetic field is done by simulation with CST Microwave studio and experimentation thanks to a 3D axis positioning system in an anechoic chamber (Figure 3). The H -field is measured with a near field probe (Langer MFA 01) positioned 5 mm above the antenna moving on a surface of 102×90 mm². The scanning starts at 10 mm away from the feeding point along the z -axis. The measurement is done by a Vector Network Analyzer (VNA) Anritsu MS4624B.

Firstly, we study the curved meander antenna without the parasitic elements. The results for the first and second resonance frequency are represented in Figures 4 and 5.

We know that the first f_1 and second f_2 modes of this antenna correspond to the dipolar and quadrupole mode respectively [21]. In Figure 4, for the first mode f_1 , we observe the evolution

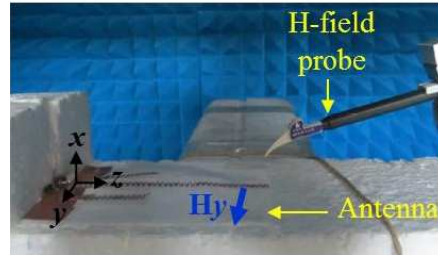


Figure 3. Experimental setup in near field measurement.

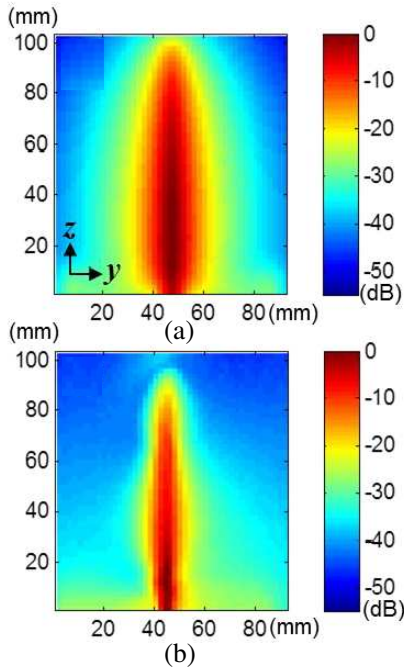


Figure 4. Field map of the component $|H_y|$ of the first dipolar mode at f_1 for the curved meander line antenna in (a) simulation and (b) measurement. Each pixel represents 4 mm^2 .

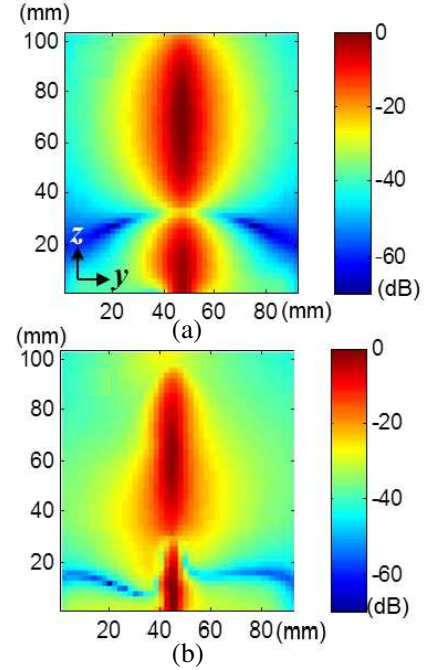


Figure 5. Field map of the component $|H_y|$ of the second quadrupole mode at f_2 for the curved meander line antenna in (a) simulation and (b) measurement. Each pixel represents 4 mm^2 .

of the magnetic field for the dipolar mode. The simulation and measurement results are in good agreement. The field amplitude is maximal at the feeding point at $z = 8 \text{ mm}$ and decreases along the radiation element. This evolution corresponds to the current evolution of a monopole antenna for dipolar mode [22]. For the second mode in Figure 5, the quadrupole mode is also represented in term of magnetic field. The field evolves along the radiating element. The field amplitude is maximum at the feeding point and decreases up to the position $z = 32 \text{ mm}$ in simulation and $z = 30 \text{ mm}$ in measurement. Then, the field amplitude increases and decreases again up to its ends. This behavior corresponds to current evolution of a quadrupole mode [22].

Secondly, we add the two parasitic elements (see Figures 1(c)–(d)). Their lengths $R1$ coincide with the position of minimum amplitude of the magnetic field at f_2 for the curved meander line antenna. The magnetic field of the new antenna is studied in simulation and in measurement for the first (Figure 6) and second (Figure 7) mode. For the first mode, this is the same behavior that the first mode of the curved meander line antenna, this is the dipole mode evolution along the monopole element. The parasitic elements are slightly seen at f_1 but with a very low level (-22 dB). The parasitic elements do not perturb the behavior of the mode. We also see that the amplitude of the mode increases, that

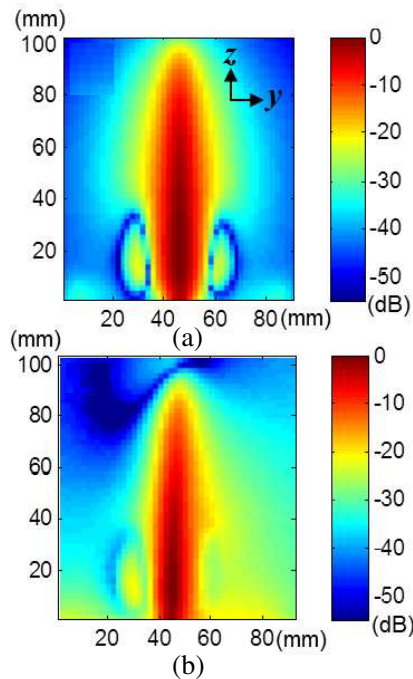


Figure 6. Field map of the component $|H_y|$ of the first mode at f_1 for the open-sleeve curved meander line antenna in (a) simulation and (b) measurement. Each pixel represents 4 mm^2 .

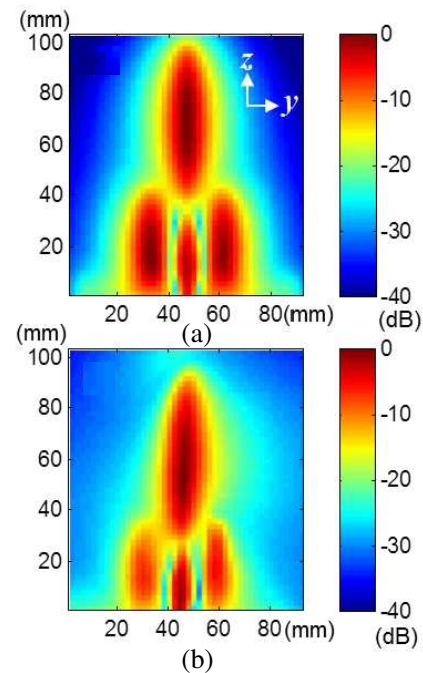


Figure 7. Field map of the component $|H_y|$ of the second mode at f_2 for the open-sleeve curved meander line antenna in (a) simulation and (b) measurement. Each pixel represents 4 mm^2 .

explains the best matching for this mode when the parasitic elements are added.

For the second mode in Figure 7, the simulation and measurement results are in good agreement. The radiating element keeps a quadrupole behavior characterized by the minimum around $z = 30 \text{ mm}$. We observe that the two parasitic elements have the same behavior that the dipolar mode, with a maximum of amplitude at the connecting point to the ground plane and it decreases to their ends. In measurement, there is an asymmetry due to experimental errors (antenna not planar, resonators not well connected...). By coupling with the monopole element, the magnetic field of the antenna can be seen as a large dipole.

3.3. Far Field Results

Then, we check in far field the radiation pattern obtained for both antennas. The radiation patterns of the antenna with and without the resonators have been measured in the anechoic chamber of *Centre Commun de Ressources en Microondes (CCRM)* [26] (Figure 8), in Marseille, France. The distance between the Antenna Under Test (AUT) and the receiver antenna is 8.4 m and both antennas are positioned at 2.5 m high. The support of the AUT is supposed transparent to electromagnetic waves in the microwave range and has an excursion in azimuth of 360° . The receiver antenna is a wideband ridged horn antenna (ARA-DRG2020/A). The measurement is realized by a VNA Anritsu MS2036C.

The radiation patterns are shown for the curved meander line antenna in Figure 9 in simulation and measurement at f_1 and f_2 . The radiation patterns at f_1 and f_2 of the open-sleeve curved meander line antenna are represented in Figure 10. In these figures, the ground plane is located at the bottom of the figures. The radiation patterns have been measured in the E -plane (yz -plane) of the antennas.

For the first mode of the two antennas (Figures 9(a) and 10(a)), radiation patterns are dipolar in simulation and in measurement. For the second mode of the curved meander line antenna (Figure 9(b)), the radiation patterns are quadrupole in simulation and in measurement like expected for the second mode of a monopole antenna. The simulation and measurement results are in good agreement, four lobes

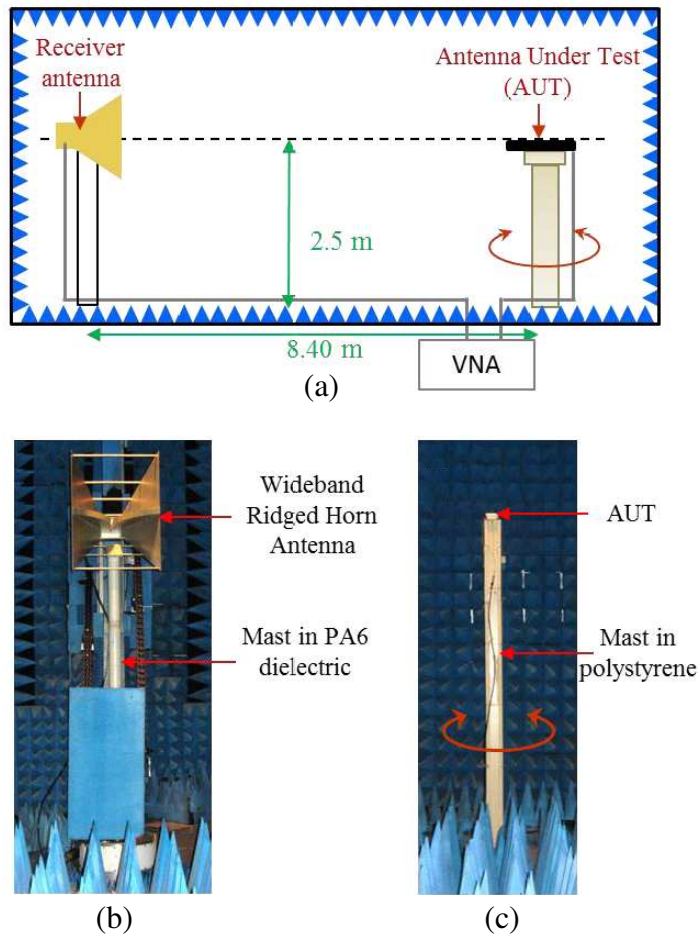


Figure 8. (a) Experimental setup in far field measurement. (b) Position of the receiver antenna. (c) Position of the AUT.

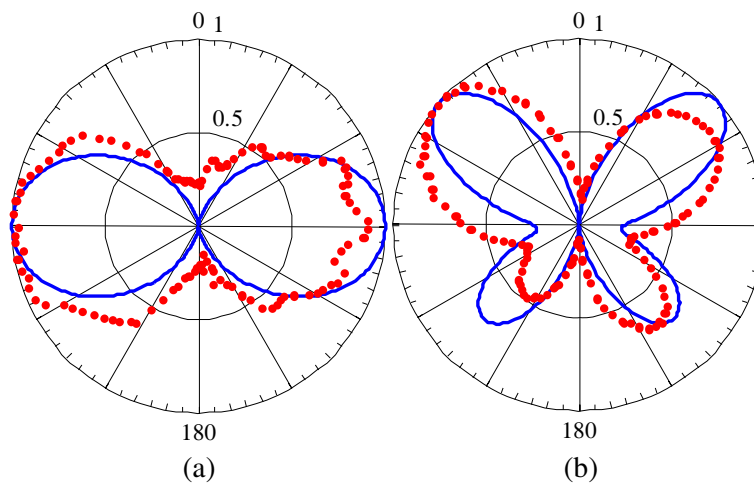


Figure 9. Radiation pattern (linear amplitude normalized to the maximum) in the E -plane of the (a) first and (b) second mode for the curved meander line antenna in simulation (blue line) and in measurement (red dashed line).

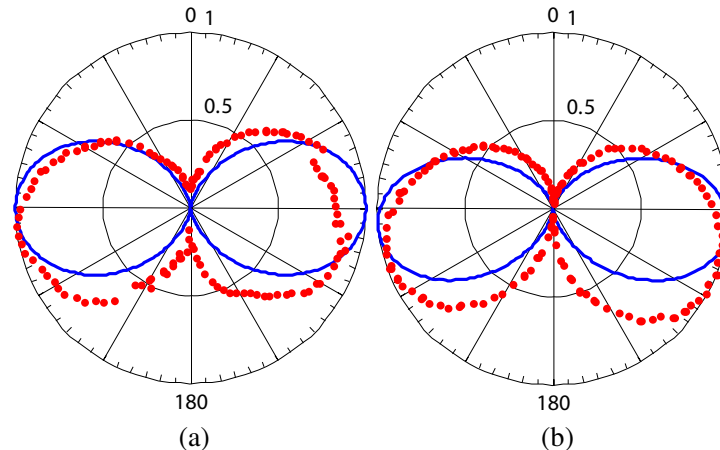


Figure 10. Radiation pattern (linear amplitude normalized to the maximum) in the E -plane of the (a) first and (b) second mode for the open-sleeve curved meander line antenna in simulation (blue line) and in measurement (red dashed line).

are represented. The radiation patterns in simulation and in measurement are asymmetric because of the ground plane. For the open-sleeve curved meander line antenna (Figure 10(b)), a dipolar radiation pattern is observed in both simulation and measurement. The lobes in simulation and measurement point out the lower part of the pattern. The differences between simulation and measurement might be due to the slightly undulated shape of the antenna consequently to its flexibility.

Effectively, the quadrupole mode of the second resonance frequency of a monopole antenna has been changed into a dipole mode by adding two parasitic elements of length matching a dipole element working at the second resonance frequency f_2 .

The 3 dB aperture angles at the first mode f_1 in measurement are quite the same with and without resonators in measurement (85° without 80° with). In simulation, the 3 dB aperture angles are the same with and without resonators (88°). For the second mode of the open-sleeve antenna, the 3 dB aperture angle (83° in measurement, 80° in simulation) is the same than the first mode. This second mode has obviously an aperture angle much more important than the quadrupole mode. This is less directive but has the same aperture angle as the first dipole mode. The main result is that the open-sleeve antenna is better matched at f_1 and f_2 with resonators and radiates more power with dipole modes. In this case, it is possible to radiate two dipole modes at two frequencies to increase the efficiency of the link budget of a transmission in free space.

4. SUMMARY AND CONCLUSIONS

In summary, we have demonstrated how to change a quadrupole mode into a dipole mode by adding two resonators of length resonating at the second mode. A dual-band antenna with two dipole modes has been realized. The study in near field permits to understand how the resonators radiate at the resonance frequencies. They can be seen in near field as two dipole elements working at the second mode. In conclusion, adding resonators of specified length permits to generate dipole sources fed by the ground plane and by coupling with the driven elements. We have realized a dual-band antenna on a flexible substrate with dipole radiations. This antenna can be easily folded and inserted in an embedded system.

ACKNOWLEDGMENT

This project is supported by the French Fonds Unique Interministériel, with the support of the Provence Alpes Côte d'Azur Region and Oséo in the context of the Belocopa project.

REFERENCES

1. Bekali, Y. K. and M. Essaidi, "Compact reconfigurable dual frequency microstrip patch antenna for 3G and 4G mobile communication technologies," *MOTL*, Vol. 55, No. 7, 1622–1626, July 2013.
2. Serra, A. A., P. Nepa, and G. Manara, "A wearable two-antenna system on a life jacket for Cospas-Sarsat personal locator beacons," *IEEE Trans. on Ant. and Propag.*, Vol. 60, No. 2, 1035–1042, February 2012.
3. Yang, L., L. Martin, D. Staiculescu, C. P. Wong, and M. M. Tentzeris, "Design and development of compact conformal RFID antennas utilizing novel flexible magnetic composite materials for wearable RF and biomedical applications," *Antennas and Propagation Society International Symposium*, July 2008.
4. De Cos, M. E. and F. Las-Heras, "Polypropylene-based dual-band CPW-fed monopole antenna," *IEEE Trans. on Ant. and Propag.*, Vol. 55, No. 3, 264–273, June 2013.
5. Zhou, J., Y. Luo, B. You, and X. J. Yan, "Novel tri-band antenna endloaded with koch fractal loops," *MOTL*, Vol. 54, No. 3, 620–623, March 2012.
6. Kim, D. O., C. Y. Kim, D. G. Yang, "Flexible Hilbert-curve loop antenna having a triple-band and omnidirectional pattern for WLAN/WiMAX applications," *International Journ. of Ant. and Propag.*, Vol. 2012, 1–9, 2012.
7. Chen, H. D., W. S. Chen, Y. T. Cheng, Y. C. Lin, "Dualband meander monopole antenna," *Proc. IEEE Antennas and Propagation Society International Symposium*, Vol. 3, 48–51, July 2003.
8. Wu, S. J., C. H. Kang, K. H. Chen, J. H. Tarn, "A multiband quasi-yagi type antenna," *IEEE Trans. on Ant. and Propag.*, Vol. 58, No. 2, 593–596, February 2011.
9. Asghar, A. M., M. Malick, M. Karlsson, and A. Hussain, "A multiwideband planar monopole antenna for 4G devices," *MOTL*, Vol. 55, No. 3, 589–593, March 2013.
10. Ali, M., M. Okoniewski, M. A. Stuchly, and S. S. Stuchly, "Dual-frequency strip-sleeve monopole for laptop computers," *IEEE Trans. on Ant. and Propag.*, Vol. 47, No. 2, 317–323, February 1999.
11. Raham, M., M. A. Stuchly, and M. Okoniewski, "Dual-band strip-sleeve monopole for handheld telephones," *MOTL*, Vol. 21, No. 2, 79–82, April 1999.
12. Li, J.-Y. and Y.-B. Gan, "Multi-band characteristic of open sleeve antenna," *Progress In Electromagnetics Research*, Vol. 58, 135–148, 2006.
13. Spence, T. G. and D. H. Werner, "A novel miniature broadband/multiband antenna based on an end-loaded planar open-sleeve dipole," *IEEE Trans. on Ant. and Propag.*, Vol. 54, No. 12, 3614–3620, December 2006.
14. Durgun, A. C., C. A. Balanis, C. R. Birtcher, and D. R. Allee, "Design, simulation, fabrication and testing of flexible bow-tie antennas," *IEEE Trans. on Ant. and Propag.*, Vol. 59, No. 12, 4425–4435, December 2011.
15. Mantash, M., A. C. Tarot, S. Collardey, and K. Mahdjoubi, "Investigation of flexible textile antennas and AMC reflectors," *International Journal of Antennas and Propagation*, Vol. 2012, 1–10, February 2012.
16. Main, Y., Q. Chen, L.-R. Zheng, and H. Tenhunen, "Development and analysis of flexible UHF RFID antennas for "Green" electronics," *Progress In Electromagnetics Research*, Vol. 130, 1–15, July 2012.
17. Paul, D. L., L. Zhang, and L. Zheng, "Flexible dual-band LCP antenna for RFID applications," *Proceedings of EMTS*, 973–976, May 2013.
18. Raad, H. R., A. I. Abbosh, H. M. Al-Rizzo, and D. G. Rucker, "Flexible and compact AMC based antenna for telemedicine applications," *IEEE Trans. on Ant. and Propag.*, Vol. 61, No. 2, 524–531, February 2013.
19. Leung, S. Y. Y. and D. C. C. Lam, "Performance of printed polymer-based RFID antenna on curvilinear surface," *IEEE Trans. on Electronics Packaging Manufacturing*, Vol. 30, No. 3, 200–205, July 2007.

20. Khaleel, H. R., H. M. Al-Rizzo, D. G. Rucker, and S. Mohan, "A compact polyimide-based UWB antenna for flexible electronics," *IEEE Trans. on Ant. and Wireless Propag. Letters*, Vol. 11, 564–567, May 2012.
21. Jackson, J. D., *Classical Electrodynamics*, 3rd Edition, John Wiley & Sons Inc., 1999.
22. Balanis, C. A., *Antenna Theory Analysis and Design*, 3rd Edition, John Wiley & Sons Inc., 2005.
23. Nicolson, A. M. and G. F. Ross, "Measurement of the intrinsic properties of materials by time-domain techniques," *IEEE Trans. on Instrum. and Meas.*, Vol. 19, No. 4, November 1970.
24. Sabouroux, P., www.epsimu.fr, 2008–2013.
25. Ba, D. and P. Sabouroux, "*EpsiMu*, a Toolkit for permittivity and permeability measurement in microwave domain at real time of all materials: Applications to solid and semisolid materials," *MOTL*, Vol. 52, No. 12, 2010.
26. Geffrin, J. M. and P. Sabouroux, "Continuing with the Fresnel database: Experimental setup and improvements in 3D scattering measurements," *Inverse Problems*, IOP Publishing, Vol. 25, No. 2, 024001, 2009.